Citation: CPT Pharmacometrics Syst. Pharmacol. (2019) 8, 676–684; doi:10.1002/psp4.12448

ARTICLE

Quantitative Systems Pharmacology Model of a Masked, Tumor-Activated Antibody

Mark Stroh[1,*], Jason Sagert[1], John M. Burke[2], Joshua F. Apgar[2], Lin Lin[2], Bjorn L. Millard[2] and W. Michael Kavanaugh[1]

PROBODY therapeutics (Pb-Tx) are protease-activatable prodrugs of monoclonal antibodies (mAbs) designed to target tumors where protease activity is elevated while avoiding normal tissue. They are composed of a parental mAb, a mask that inhibits antibody binding to target, and a protease-cleavable substrate between the mask and the mAb. We report a quantitative systems pharmacology model for the rational design and clinical translation of Pb-Tx. The model adequately described monkey pharmacokinetic data following the administration of six anti-CD166 Pb-Tx of varying mask strength and substrate cleavability and captured the trend of decreasing Pb-Tx systemic clearance with increasing mask strength. Projections to humans suggested both higher levels of Pb-Tx in tumor relative to parental mAb and an optimal mask strength for maximizing tumor receptor–mediated uptake. Simulations further suggested the majority of circulating species in humans would be intact/masked Pb-Tx, with no significant flux of cleaved/activated species from tumor to the systemic compartment.

Study Highlights

WHAT IS THE CURRENT KNOWLEDGE ON THE TOPIC?
☑ The therapeutic utility of a given monoclonal antibody (mAb) is impacted by its distribution. PROBODY therapeutics (Pb-Tx) are prodrug forms of mAb that are designed to activate preferentially in diseased tissue. Although the science of mAb distribution is mature, there are no published model-based approaches for extrapolation to the case of Pb-Tx.

WHAT QUESTION DID THIS STUDY ADDRESS?
☑ Here we report a quantitative systems pharmacology (QSP) model to integrate the effect of both prodrug and system properties on Pb-Tx pharmacokinetics (PK)/pharmacodynamics (PD) for the rational design and clinical translation of Pb-Tx.

WHAT DOES THIS STUDY ADD TO OUR KNOWLEDGE?
☑ Here we report the first QSP model for a Pb-Tx that incorporates provisions both unique to the Pb-Tx and common to the historical database for mAb PK/PD. Using a family of Pb-Tx directed against CD166, the QSP Pb-Tx model provides a model-based proof of principle for Pb-Tx in the case of a target expressed on both in healthy tissue and in the tumor. The QSP Pb-Tx model predictions suggest higher levels of Pb-Tx in the tumor relative to parental mAb and suggest that receptor-mediated uptake in tumor relative to peripheral tissues may be tuned with mask strength. The QSP Pb-Tx model further suggests that the predominant circulating species in humans would be intact Pb-Tx, with no significant contribution of cleaved species from tumor to the systemic.

HOW MIGHT THIS CHANGE DRUG DISCOVERY, DEVELOPMENT, AND/OR THERAPEUTICS?
☑ This study suggests that model-informed drug development can be used to customize Pb-Tx distribution to maximize exposure at desired sites of action while sparing healthy tissue.

Monoclonal therapeutic antibodies (mAbs) have ushered in a new era in medicine, now offering treatment options across multiple therapeutic areas.[1] Because the mechanism of action for mAbs involves binding antigens, the therapeutic window for mAbs is coupled to the distribution of the target. The differential expression of target antigens on normal and diseased tissue acts to widen the window, whereas broad distribution risks undesired action in healthy tissue. PROBODY therapeutics (Pb-Tx) are prodrug forms of mAbs that are designed to restrict the distribution of activated mAbs to diseased tissue.[2] The Pb-Tx is as illustrated in **Figure 1** and is composed of (i) a parental mAb directed to antigens and (ii) a prodomain. The prodomain is in turn composed of a mask that inhibits the binding of the parental mAb to an antigen and a protease-cleavable substrate that is inserted between the mask and the light chain of the parental mAb. The mask physically reduces the ability of the Pb-Tx to bind to the target antigen through interaction/binding of the mask with the paratope of the antibody. For a cancer Pb-Tx, the substrate may be cleaved by tumor-associated proteases such that when the substrate is cleaved the mask is then preferentially released in the tumor relative to the systemic

[1]CytomX Therapeutics, Inc., South San Francisco, California, USA; [2]Applied BioMath, Lincoln, Massachusetts, USA. *Correspondence: Mark Stroh (mstroh@cytomx.com)
Received: February 7, 2019; accepted: May 29, 2019. doi:10.1002/psp4.12448

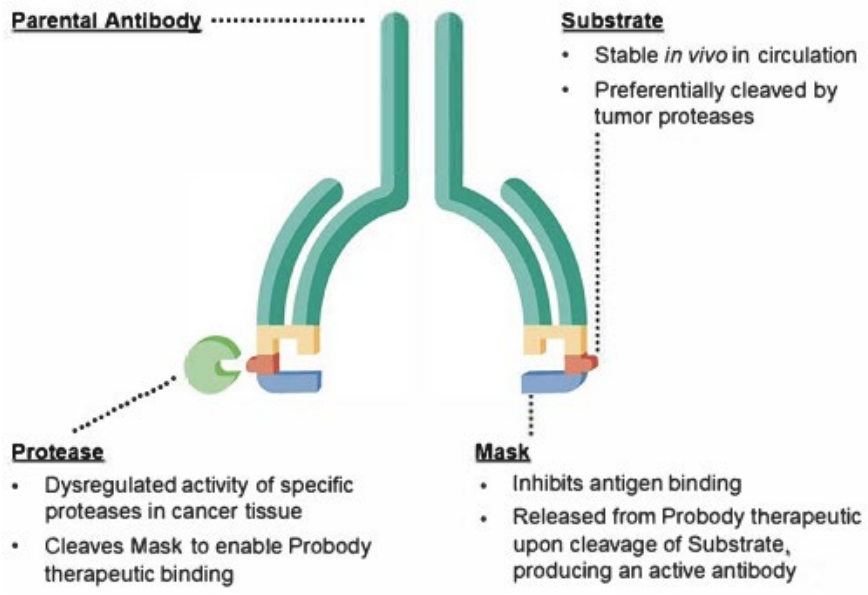

Figure 1 Structure of a PROBODY therapeutic. A PROBODY therapeutic is a prodrug form of a monoclonal antibody and is composed of a parental monoclonal antibody and a prodomain. The prodomain is composed of a mask that inhibits binding to an antigen and a protease-cleavable substrate between the mask and the light chain of the monoclonal antibodies.

compartment; this results in local activation of the Pb-Tx at the intended site of action and, subsequently, an enhanced therapeutic index in nonclinical models.[2] Pb-Tx can be "tuned" for a particular application by varying the strength of the mask, the cleavability of the substrate, and the affinity of the parental antibody.

To fully recognize the therapeutic benefit of Pb-Tx, it becomes necessary to understand not only Pb-Tx distribution following administration but also the distribution of its activated forms. The determinants of mAb distribution both in the systemic compartment[3,4] and in the tumor[5] are well known. However, these events occur downstream of Pb-Tx administration, distribution, and activation by proteases. The rational design of Pb-Tx is a multidimensional problem at the level of the drug (e.g., mAb affinity, masking strength, and substrate stability) and the system (e.g., protease activity, receptor density, tumor perfusion rate, partition coefficient, and volume). A quantitative systems pharmacology (QSP) approach provides a means to capture and query our current understanding of how the properties of the drug and system interact to affect Pb-Tx distribution.[6] The aim of this investigation is to develop a QSP model for the rational design and clinical translation of Pb-Tx that describes how different drug and system properties collectively impact pharmacokinetics (PK) and pharmacodynamics of Pb-Tx (QSP Pb-Tx model).

The Pb-Tx selected for this investigation was directed against activated leucocyte adhesion molecule (ALCAM or CD166). CD166 is a cell adhesion molecule highly expressed in multiple cancer types, making it an attractive target for therapy. However, its expression on many cell types in healthy tissue (including activated leukocytes, neurons, and epithelial and endothelial cells) is problematic for traditional mAb approaches. A Pb-Tx approach is ideally suited for such targets, and a Pb-Tx directed against CD166 and conjugated to the cytotoxin DM4 is currently under clinical investigation in a variety of different cancer indications (CX-2009, ClinicalTrials.gov identifier NCT03149549).

MATERIALS AND METHODS

PK study for anti-CD166 Pb-Tx in cynomolgus monkeys

All animals were housed, maintained, and treated in accordance to standard ethical animal handling guidelines. The study was reviewed and approved by the Institutional Animal Care and Use Committee at Charles River Laboratories. Experimentally naive cynomolgus monkeys were randomly assigned to dosing groups (n = 2 per group) at Charles River Laboratories. The test articles were administered at 3, 5, and 10 mg/kg via intravenous (slow bolus) injection. Whole blood was obtained from each unanesthetized animal for up to 21 days postdose. Pb-Tx and mAb concentrations in the cynomolgus monkey lithium heparin plasma samples were determined using sandwich-based colorimetric enzyme-linked immunosorbent assay methods.

QSP Pb-Tx model construction

A QSP model was developed based on known mechanisms of Pb-Tx breathing, cleavage, first-order plasma elimination, tissue and tumor biodistribution, receptor binding, and receptor and receptor–drug complex endocytosis.

All models were implemented using KroneckerBio version 0.4. Simulation runs, parameter estimation, and parameter scans were performed using MATLAB version 2015b (Mathworks, Natick, MA). KroneckerBio is open-source software and is maintained at https://github.com/kroneckerbio. The version of KroneckerBio used for these simulations was tested prior to use and is archived by Applied BioMath (Lincoln, MA).

Kronecker describes the systems as a system of ordinary differential equations with the following form:

$$\frac{dx}{dt} = k + Ax + B(x \otimes x)$$

where k is a vector of zero-order rate constants, A is an n by n matrix of first-order rate constants, and B is an n by n matrix of second-order rate constants. The values of these matrices are provided as model code in **Supporting Information**.

Calibration against cynomolgus monkey data

The model was calibrated to PK data following administration of anti-CD166 Pb-Tx with varying mask and substrate characteristics. In addition to the parental anti-CD166 mAb ($mAb_{0,0}$), four Pb-Tx derived from $mAb_{0,0}$ with different substrates (designated as S1 and S2, respectively) and masks (designated M1 and M2, respectively) were investigated (designated as $Pb\text{-}Tx_{M1,S1}$, $Pb\text{-}Tx_{M2,S1}$, $Pb\text{-}Tx_{M1,S2}$, and $Pb\text{-}Tx_{M2,S2}$, respectively). In addition, one Pb-Tx did not have a protease-activating substrate and is designated as $Pb\text{-}Tx_{M1,0}$. The estimation was done simultaneously for all six molecules assuming that the physiologic model parameters (plasma volume, target expression, etc.) and the parameters that describe the common molecular features (mono-valent binding affinity of the open or cleaved Pb-Tx, first-order elimination rate, central to peripheral distribution rates) were constant across molecules. The parameters that describe the differences between the molecules governing mask strength and cleavage rate (i.e., K_{mask} and k_{cleave}, respectively; see Results) were estimated as follows: First, the simulations were run over a range of parameter values for the parameters K_{mask} and k_{cleave}. The simulations were compared with the data, and the negative log likelihood function was computed. As described further in the Results, given the results of the parametric study of K_{mask} and k_{cleave}, K_{mask} for M1 and M2 were first estimated while holding k_{cleave} for S1 and S2 to a fixed value. The k_{cleave} for S1 and S2 were then estimated by fixing K_{mask} for M1 and M2 to the value of the previous step.

RESULTS

QSP Pb-Tx model construction

The proposed QSP Pb-Tx model captures events both at the (i) Pb-Tx and the (ii) compartmental levels; at each level, the QSP Pb-Tx model has both provisions that are unique to the Pb-Tx and those that are shared with other mAb pharmacology models. The schematic for events at the Pb-Tx level is provided in **Figure 2a**. The Pb-Tx is depicted first as an intact moiety with two masks, with subsequent successive stages of irreversible cleavage reactions characterized by a pseudo first-order rate constant k_{cleave} (1/second) that captures both the rate of substrate proteolysis and protease concentration. The first and second cleavage reactions generate the mono-cleaved Pb-Tx species and subsequently the dual-cleaved, parental mAb, respectively. In addition, reversible "breathing" reactions that reflect mask binding and unbinding to the mAb are included for all but the dual-cleaved parental mAb. Breathing reactions are expressed in terms of a ratio (K_{mask}) of first-order rate constants for mask closing (1/second) and opening (1/second). The intact Pb-Tx species with both masks closed does not bind target; both the mono-cleaved Pb-Tx with one mask closed and intact Pb-Tx with one mask open exhibit monovalent binding to target. The species on the diagonal of **Figure 2a** are Pb-Tx with combinations of breathing and/or cleavage reactions that result in both arms available for bivalent binding. The species of **Figure 2a** distribute to plasma, peripheral, and tumor compartments as depicted in **Figure 2b**. All free Pb-Tx species are assumed to be eliminated from the plasma compartment at the same first-order rate constant k_{el} (1/second). Plasma Pb-Tx species equilibrate with the peripheral compartment with intercompartment transport rate constants k_{12} (1/second) and k_{21} (1/second), respectively. Plasma Pb-Tx species may further distribute to the tumor compartment with intercompartment transport rate constants k_{13} (1/second) and k_{31} (1/second), respectively; k_{13} (1/second) and k_{31} (1/second) are further derived from a plasma to tumor steady-state Pb-Tx concentration ratio (partition coefficient, p) and a plasma to tumor perfusion rate (Q (1/second)). Based on internal (data not shown) and human protein atlas data,[7] model provisions were included for binding to target within the peripheral and tumor compartments. Within both peripheral and tumor compartments, monovalent and bivalent Pb-Tx species bind target with forward rate k_{on1} (1/(nM*second)), and both k_{on1} and k_{on2} (1/(nM*second)), respectively, and reverse rate constant k_{off1} (1/second). The forward rate k_{on1} was assumed from the literature,[8] and k_{on2} was estimated under the assumption that avidity is not influential. Target expression in both the periphery and tumor are governed by target synthesis and endocytosis rate constants k_{synR} (nmol/second) and k_{endo} (1/second), respectively, and can be further expressed as receptor per cell[9] (see **Table 1**). Additional details are provided in the Methods.

Calibration against cynomolgus monkey data

The QSP Pb-Tx model was next calibrated to fit cynomolgus monkey PK data following administration of one mAb and five Pb-Tx to cynomolgus monkeys. Dose levels investigated included 3, 5, and 10 mg/kg administered either as a single dose or as two doses administered 3 weeks apart.

Parameter scans were conducted to compute the negative log likelihood of K_{mask} and k_{cleave} given the data for each molecule; parameters other than K_{mask} and k_{cleave} were set to the values in **Table 1**. The negative log likelihood following a parametric study of K_{mask} and k_{cleave} is provided in **Figure S1**. From **Figure S1a**, a one-sided lower bound could be determined for K_{mask} for M1, and a two-sided bound for K_{mask} for M2 was observed. From **Figure S1b**, an upper bound on k_{cleave} was identified from the marginal probability plot, but no lower bound could be determined (i.e., it could not be distinguished from zero). To get refined estimates of K_{mask} as well as the upper bound of k_{cleave}, K_{mask} was estimated by fitting the model to the PK data while fixing k_{cleave} for S1 and S2 to zero. The estimates of K_{mask} for M1 and M2 were consistent with fluorescence-activated cell sorting (FACS) binding

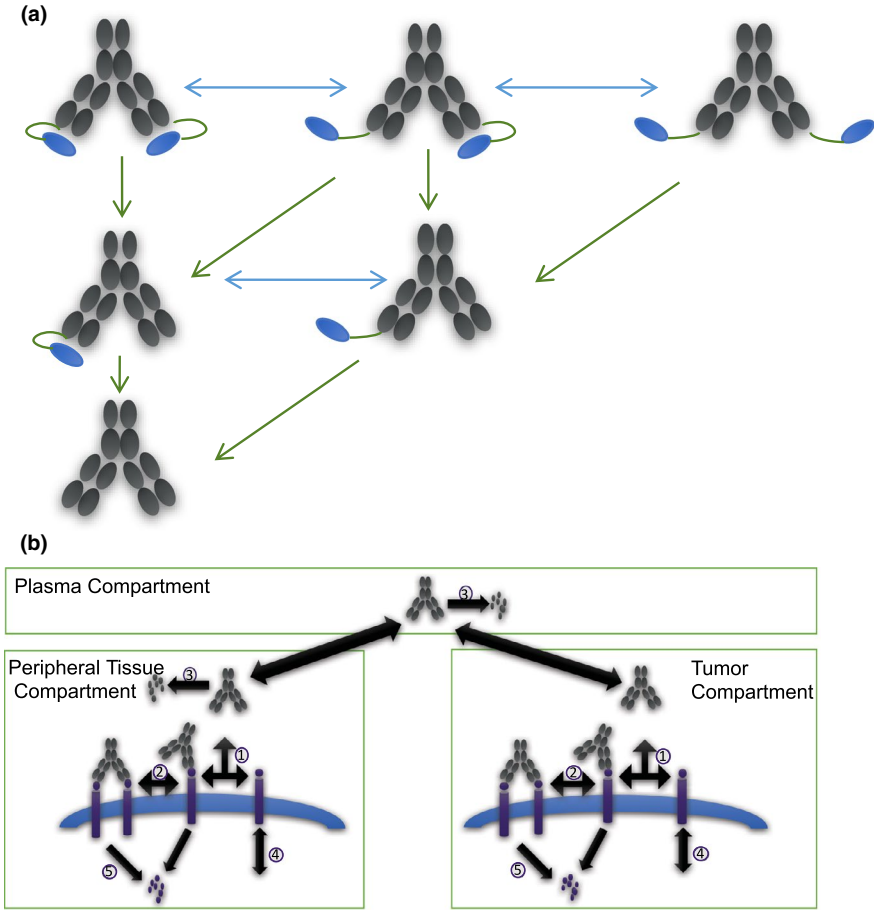

Figure 2 The quantitative systems pharmacology Pb-Tx model. The quantitative systems pharmacology Pb-Tx model captures events both at Pb-Tx and compartmental levels. (**a**) At the Pb-Tx level, reversible breathing events (represented by bidirectional arrows) and irreversible cleavage reactions (represented by unidirectional arrows) are both captured in the model. (**b**) Concurrently, all six forms of the Pb-Tx distribute to the plasma, peripheral, and tumor compartments. In the peripheral and tumor compartments, a subset of Pb-Tx may engage in monovalent (1) or bivalent (2) binding, depending on the number of breathing or cleaved binding sites, respectively. Circulating Pb-Tx and unbound Pb-Tx in the peripheral compartment (3) and internalized Pb-Tx (5) may all be eliminated. Pb-Tx, PROBODY therapeutics.

data (see Discussion) and were close to (but still above) the lower bound for M1 identified from marginal probability and similar to the isolated minima for M2, respectively. The one-sided bound for K_{mask} for M1 suggested that M1 was indistinguishable from a nonbinding molecule. For the parental antibody $mAb_{0,0}$ (with no mask group), the marginal probability suggested that the mask strength had to be very low, which is consistent with the molecule not having a masking group. The K_{mask} was then fixed to the value for M1 and M2 (as appropriate), and then the value of k_{cleave} was searched to find the largest value that still gave an acceptable fit to the PK data for all simulations. The k_{cleave} estimated for the parental antibody $mAb_{0,0}$ was a one-sided distribution with only very high rates being likely, consistent with $mAb_{0,0}$ lacking a masking group. Because different substrates could not clearly be distinguished from the PK data, the value of k_{cleave} for S1 and S2 was constrained to be equal. The marginal probabilities for the S1 and S2 substrates were indistinguishable from an uncleavable substrate; although a value of $k_{cleave} = 0$ was consistent with the data, values of $k_{cleave} <$ 3e-7 1/second still produced acceptable fits, and 3e-7 1/second represented an upper bound on this value. This value of 3e-7 1/second was carried forward as the likely maximum value for k_{cleave}.

Figure 3 suggests an adequate fit of the QSP Pb-Tx model to observed monkey PK data across the dose levels, mask strengths, and substrates entered into the evaluation. Most notably, across all dose levels, the observed data exhibited the hallmark evidence of target-mediated drug disposition (TMDD) for the parental $mAb_{0,0}$, which was captured by the QSP Pb-Tx model. At the 3 mg/kg dose level, the observed data suggested decreased importance of TMDD in the disposition of the Pb-Tx species overall, with evidence of TMDD minimized both for Pb-Tx species with noncleavable substrate ($Pb\text{-}Tx_{M1,0}$) and highest mask strength ($Pb\text{-}Tx_{M1,S1}$ and $Pb\text{-}Tx_{M1,S2}$). These overall trends were again evident at the 5 mg/kg and 10 mg/kg dose levels, where the contribution of TMDD was lessened for the Pb-Tx species of successively higher mask strengths; with k_{cleave} held fixed to the upper bound of 3e-7 1/second, varying K_{mask} alone was sufficient for the QSP Pb-Tx model to capture trends overall.

Table 1 Parameters in the monkey QSP model

Parameter	Value	Notes	Reference
Body weight (kg)	2.6	Fixed based on its typical value in the literature	15
Plasma and peripheral volumes, V_1 and V_2, respectively (L)	0.1	Fixed based on its typical value in the literature	16
First-order elimination rate, k_{el} (1/second)	1.0e-6	From fit to beta-phase PK data	—
Target endocytosis rate constant, k_{endo} (1/second)	1.0e-4	Typical value for receptor turnover rate	17
Target synthesis rate, k_{synR} (nmol/second)	9.0e-5	k_{synR} is estimated directly by fitting the model to PK data. This would correspond to an approximate RPC estimate of 1e4/cell, which is in the typical range of receptor expression (1e3-1e6/cell), where RPC = k_{synR}/k_{endo} • 1e-9 • Avog/Ncell Avog = Avogadro's number And Ncell = 4e10, where Ncell in monkey is based on the estimated Ncell in humans (3% of total cells or 1e12) and scaled to monkey by the ratio of body weights in monkey and human	17
Intercompartment transport rate constant, k_{12} (1/second)	1.1e-5	From fit to alpha-phase PK	—
Intercompartment transport rate constant, k_{21} (1/second)	1.0e-5		
Apparent binding affinity for parental monoclonal antibody, K_{app} (nM)	1.0		
Forward binding rate, k_{on1} (1/(nM*second)	1e-3	Set equal to a standard value from the literature	8
Forward binding rate, k_{on2} (1/(nM*second))	1e-3	k_{off1} is a derived quantity based on k_{on1} and K_{app} as follows: $k_{off1} = k_{on1} \bullet K_{app}$	—
Reverse binding rate constant, k_{off1} (1/second)	2e-3		
Fold-masking, K_{mask}	57 (M2) 220 (M1)	From fit of PK using parametric scan	—
Rate constant for cleavage reaction, k_{cleave} (1/second)	<3e-7		

PK, pharmacokinetics; QSP, quantitative systems pharmacology; RPC, receptor per cell.

Human QSP Pb-Tx model

Following calibration against monkey PK data, the QSP Pb-Tx model was used to project human PK under a series of assumed values for the drug (e.g., K_{mask}) and the tumor (e.g., Q and receptor concentration (R_T (nmol))); fold increases in k_{cleave} for the tumor relative to the systemic compartment was also varied to implicitly capture the effect of both drug (substrate stability) and tumor (protease activity) properties on PK. As described further in the Methods, elementary rate constants (e.g., k_{endo}, k_{on1}, k_{on2}, k_{off}) and normal tissue receptor concentration were assumed equal between monkey and human. Likewise, k_{cleave} was assumed to have an upper bound of 3e-7 1/second. The PK parameters k_{12}, k_{21}, and k_{el} (1/second) were scaled using allometry, and k_{13} and k_{31} were derived using the corresponding expressions in **Table 2**. These and other parameter values used in human PK projection are likewise summarized in **Table 2**.

Figure 4a,b illustrates the model-predicted PK profiles in plasma and periphery following a single 4.5 mg/kg dose of parental mAb and Pb-Tx species of increasing K_{mask}. In both compartments, the parental mAb exposure is reduced relative to total Pb-Tx, with evidence of a monotonic decrease in the terminal elimination rate with increasing K_{mask}. This observation is consistent with **Figure 4d**, where model-predicted uptake in the periphery trends lower overall with increasing K_{mask}, suggesting decreased contribution of TMDD in the periphery to the overall Pb-Tx clearance with increasing K_{mask}. The tumor compartment (**Figure 4c**) follows trends of increasing exposure and decreasing terminal elimination rate with increasing K_{mask}, respectively. **Figure 4e** suggests the relationship of increasing K_{mask} on receptor-mediated uptake in the tumor is not monotonic and instead may pass through an optimum. Following the multiple-dose administration of 3 mg/kg of Pb-Tx, from **Figure 5** the QSP Pb-Tx model suggests that the intact Pb-Tx comprises the majority of the total circulating species in the plasma.

DISCUSSION

The aim of this work was to integrate the effect of both Pb-Tx and system properties for the rational design and clinical translation of Pb-Tx directed against CD166. A fit-for-purpose approach was used to derive and inform the QSP model as a means to this end. The parameters from multiple *in vitro* and *in vivo* contexts were combined to inform the full parameter set. In instances where parameters were estimated, a stepwise approach was used because no single study was available to derive all estimated parameters. From **Table 1**, the parameters governing the cynomolgus PK that were not dependent on binding to target (e.g., k_{12}, k_{21}, and k_{el}) were estimated as one common set across all data. The parameters governing the interaction of Pb-Tx and mAb with target were either assumed

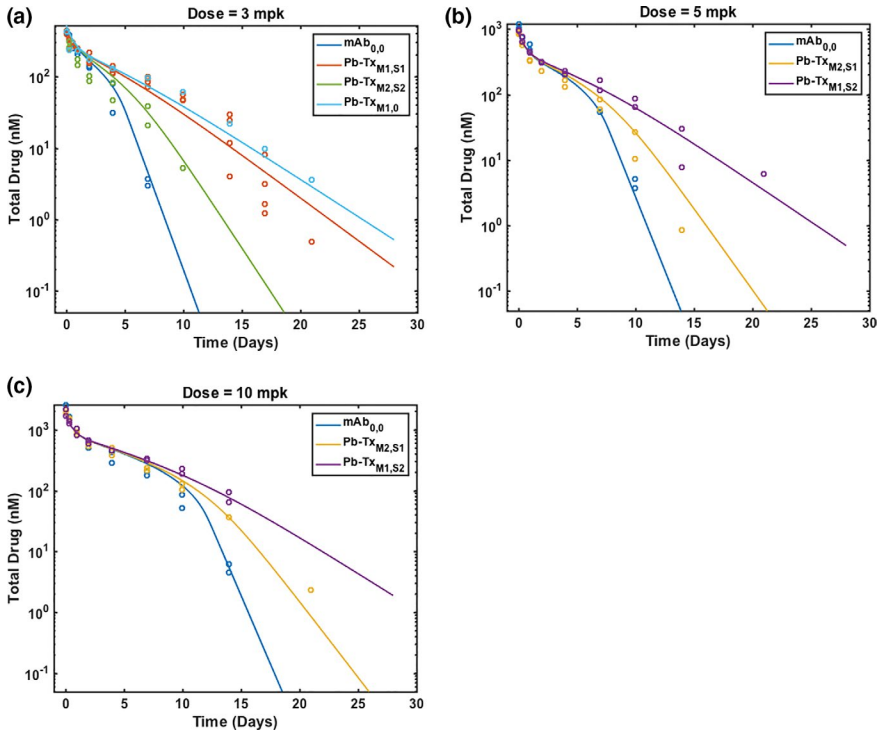

Figure 3 Model calibration (model predictions as solid lines) against observed pharmacokinetic data (hollow points) for indicated Pb-Tx administered to cynomolgus monkeys at the (**a**) 3 mg/kg, (**b**) 5 mg/kg, and (**c**) 10 mg/kg dose levels. Figure legends indicate information pertaining to mask (e.g., M1 and M2) and substrate (e.g., S1 and S2). mAb, monoclonal antibody; Pb-Tx, PROBODY therapeutics.

(e.g., k_{on1}, k_{endo}), derived based on apparent *in vitro* binding affinity (e.g., k_{on2}, k_{off1}), or further estimated from available PK data (e.g., k_{synR}, K_{mask}, k_{cleave}). To explore the possible effect of parameter uncertainty, simulations were conducted to evaluate if QSP model predictions were sensitive to selected parameters. This simulations-based exercise suggested that QSP model predictions for monkey PK were relatively sensitive to K_{mask}; however, k_{cleave} was less influential for values up to 3e-7 1/second. This provided a one-sided bound for k_{cleave} that would further provide a conservative estimate of the fraction of Pb-Tx circulating as intact. **Figure 3** suggests that the model performance was adequate given the intended use of the model.

The QSP Pb-Tx model provides both proof of principle for the enhanced therapeutic window offered by the Pb-Tx relative to the parental mAb as well as a platform to rationally maximize this window. At a given dose level in the monkey, observed data and model predictions were consistent in illustrating both reduced exposure of circulating levels of parental mAb relative to the Pb-Tx and trending of increasing Pb-Tx exposure with increasing K_{mask}. The results in the monkey further suggest that molecules sharing elements such as a given substrate or mask could be described by a common estimate of k_{cleave} and K_{mask}, respectively. These results support both the validity of these model parameters as mechanistic and the decomposability of the substrate and mask as independent design elements for the Pb-Tx. This finding implies that the masking strength (as captured through K_{mask}) estimated for one Pb-Tx with a particular mask adequately describes the mask strength of another Pb-Tx with the same mask. The K_{mask} estimates were consistent with the *in vitro* measurement determined by FACS. The K_{mask} for M2 was estimated to be 57-fold, and this was within approximately 2-fold of the *in vitro* value estimate determined from FACS (120-fold). The K_{mask} for M1 was estimated to be 220-fold, and this was similar to the FACS estimate of the 232-fold. Moreover, although observed trends in monkey provide indirect evidence that circulating Pb-Tx escape binding to a peripheral target, the consistency of these observations with predictions of the QSP Pb-Tx model corroborate this mechanism for decreased clearance.

Projections to human cancer patients depend both on a set of linked kinetic processes that govern the system and characteristics that modulate Pb-Tx binding to the target. Starting first with systemic levels of Pb-Tx, **Figure 4a** suggests a decreased systemic clearance of Pb-Tx relative to parental mAb; **Figure 4b,c** in turn suggests correspondingly increased exposure of Pb-Tx in the periphery and tumor, respectively, which equilibrate with circulating levels of Pb-Tx. Furthermore, **Figure 4a** suggests that predicted changes in Pb-Tx exposure in plasma would trend with K_{mask} in human cancer patients because of the decreased contribution of TMDD to the overall Pb-Tx clearance with increasing K_{mask}. Given the enhanced circulating levels of Pb-Tx with increasing K_{mask}, **Figure 4b,c** suggests that model-predicted Pb-Tx levels in the periphery and tumor likewise increase with K_{mask}. Key steps in the

Table 2 Parameters in the human QSP model

Parameter	Value	Notes	Reference
Body weight (kg)	70	Fixed based on its typical value in literature	15
Plasma volume, V_1 (L)	2.6	Fixed based on its typical value in literature	16
Tumor volume, V_3 (L)	0.01	Based on breast tumor	18,19
First-order elimination rate constant, k_{el} 1/(second)	6.3e-7	k_{el} is scaled by (BW_human/BW_monkey)$^{0.85}$•(V_monkey/V_human), where BW_human and BW_monkey are body weights for human and monkey, respectively, and V_monkey and V_human are the volumes of distribution for human and monkey, respectively	20
Target endocytosis rate constant, k_{endo} (1/second)	1.0e-4	Same as monkey	—
Target synthesis rate, k_{synR} (nmol/second) peripheral	2.3e-3	Obtained by $k_{synR} = k_{endo} \bullet R_T$, and where R_T is the receptor concentration and R_T is scaled by compartment volume	—
Target synthesis rate, k_{synR} (nmol/second) tumor	2.7e-4	Obtained by $k_{synR} = k_{endo} \bullet R_T$	—
Intercompartment transport rate constant, k_{12} (1/second)	4.8e-6	Allometric scaling: k_{12} and k_{21} are scaled by (BW_human/BW_monkey)$^{(-0.25)}$	15
Intercompartment transport rate constant, k_{21} (1/second)	4.4e-6		
Intercompartment transport rate constant, k_{13} (1/second)	1.9e-8	k_{13} and k_{31} are obtained as follows: $k_{13} = Q \bullet p/(p + V_1/V_3)$ $k_{31} = Q/(1 + p \bullet V_3/V_1)$, where Q is plasma to tumor perfusion rate 1e-5 1/second, and p is partition coefficient 0.5. The Q and p values are within the range of literature estimates	11–14
Intercompartment transport rate constant, k_{31} (1/second)	1.0e-5		
Forward binding rate, k_{on1} (1/(nM*second))	1e-3	Assumed to be the same as monkey	—
Forward binding rate, k_{on2} (1/(nM*second))	1e-3		
Reverse binding rate constant, k_{off1} (1/second)	2e-3		
Fold-masking, K_{mask}	57 (M2) 220 (M1)	Assumed to be the same as monkey	—
Rate constant for cleavage reaction, k_{cleave} (1/second)	<3e-7	Assumed to be the same as monkey for central and peripheral compartments	—

QSP, quantitative systems pharmacology.

mechanism of action for antibody drug conjugates involve first binding of the antibody to its target antigen on the cell surface followed by internalization and processing of the antibody drug conjugate to release its cytotoxic payload.[10] Accordingly, it is important to next consider the amount of Pb-Tx undergoing receptor-mediated uptake in peripheral and tumor tissues as this would be expected to be a determinant of the putative therapeutic window for a PROBODY drug conjugate. Although a contrast of **Figure 4d,e** suggests higher amounts overall of Pb-Tx undergoing receptor-mediated uptake in the periphery relative to tumor, respectively, the Pb-Tx uptake per gram would be expected to be far higher for the tumor (assuming approximately a 10-mg tumor in a 70-kg patient). The composite parameter k_{cleave} captures both substrate stability and protease activity; because k_{cleave} was not uniquely identifiable in our analysis, various fold changes in k_{cleave} in the tumor relative to the periphery were considered for these simulations. Under the scenario of a 10-fold increased k_{cleave} in the tumor relative to the periphery, **Figure 4d** suggests that receptor-mediated uptake of Pb-Tx in the periphery would decrease with increasing K_{mask}, whereas **Figure 4e** suggests that this relationship in the tumor would be concave-down and pass through a maxima. The concave-down relationship between the receptor-mediated uptake in tumor and K_{mask} reflects the tradeoff of elevated amounts of total Pb-Tx in the tumor and decreased availability of species available for the binding target via breathing reactions that both come with high K_{mask}.

Projected levels of circulating Pb-Tx suggest that intact Pb-Tx comprises the majority of circulating species. This is consistent with preferential activation of Pb-Tx by tumor-associated proteases and the observation that the net flux of cleaved species from tumor over a range of assumed folds increased k_{cleave} in the tumor relative to periphery remained at or near zero (**Figure S2**). Because proteases are involved in several different diseases and conditions, it is possible that a Pb-Tx designed for cancer might also be activated in a patient who has a coexisting condition that also involves significant protease activity. However, evidence suggests that protease activity in some common conditions may not significantly contribute to Pb-Tx activation. The stability of Pb-Tx in the collagen-induced arthritis mouse model, the most commonly studied autoimmune model of rheumatoid arthritis, has suggested no increase of Pb-Tx activation compared with that in healthy control mice (unpublished data).

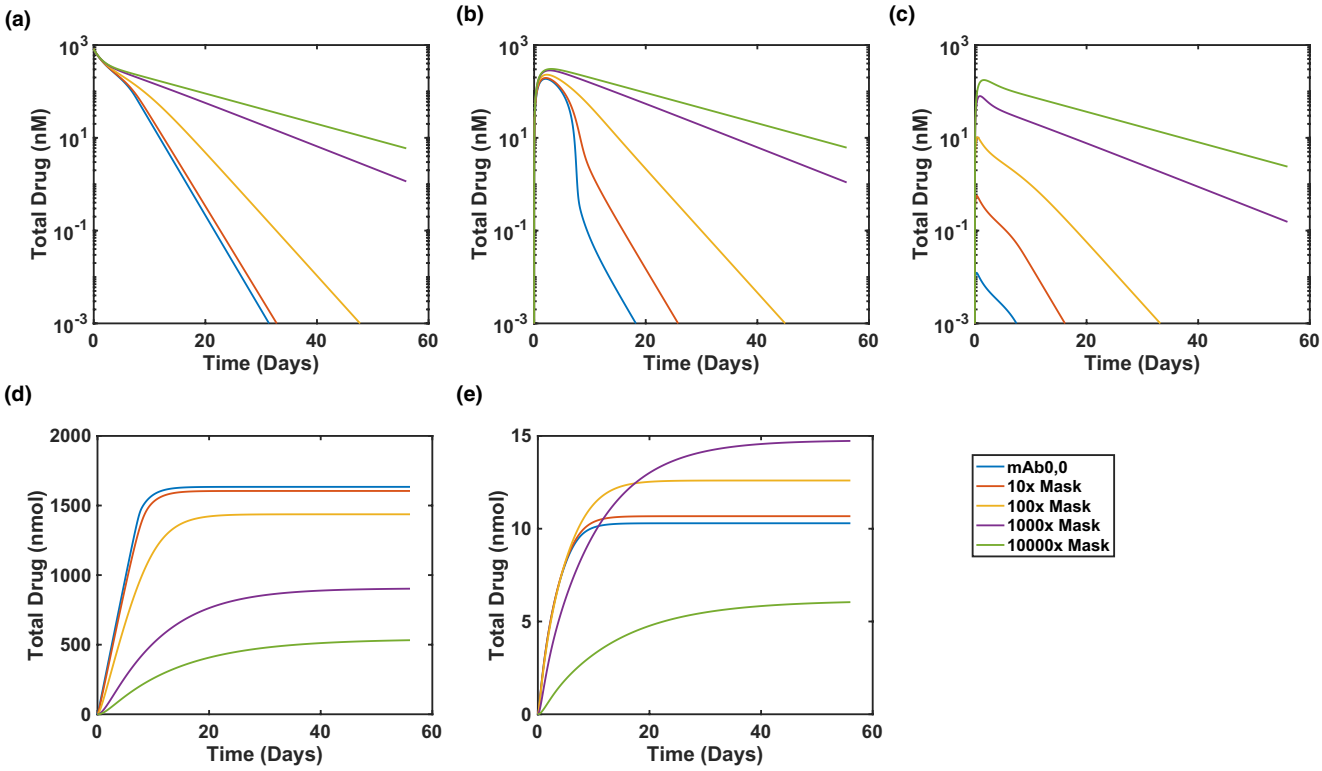

Figure 4 Human pharmacokinetic projections. Model-predicted pharmacokinetic profiles in (**a**) plasma and (**b**) periphery (**c**) tumor and receptor-mediated uptake in (**d**) periphery and (**e**) tumor following a single 4.5 mg/kg dose of parental mAb and PROBODY therapeutics of increasing mask strength (legend). mAb, monoclonal antibody.

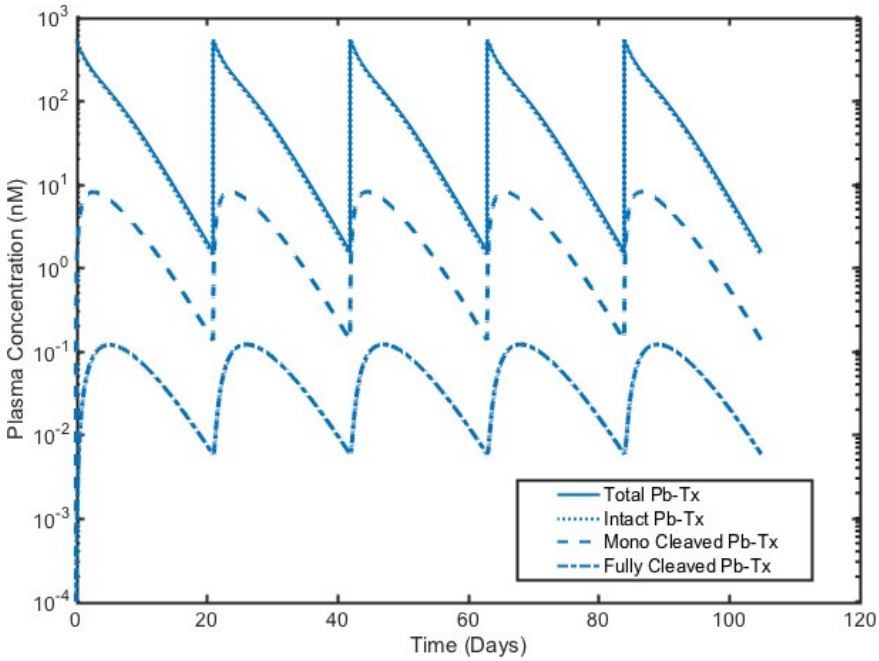

Figure 5 Projected circulating levels of total, intact, and cleaved Pb-Tx species (legend) following multiple-dose administration of 3 mg/kg of Pb-Tx to cancer patients. Pb-Tx, PROBODY therapeutics.

Depending on the intended use, this fit-for-purpose QSP Pb-Tx model can be further refined both in terms of the model parameters and in terms of the structural model. Regarding the model parameters, informing k_{on1}, k_{on2}, and k_{off} from a suitable *in vitro* assay could theoretically help to inform the QSP model. However, from **Figure 2a**, the

Pb-Tx undergoes breathing and/or cleavage reactions that result in a combination of monovalent and bivalent species available for binding to target, complicating the estimation of these parameters from an *in vitro* assay. Similarly, the availability of robust estimates for k_{endo} for CD166 in particular could help better inform the system-specific components of the model. Likewise, although available binding data with different cell lines suggested similar apparent affinities (data not shown), a further exploration of the binding affinities across a greater range of known target densities would help to further evaluate the possible importance of avidity for this system. Regarding the structural model, there are opportunities for both greater parsimony and more fully mechanistic treatment depending on the intended further use of the model. For example, although the full TMDD model as invoked in the QSP Pb-Tx model was well suited to the intended use of informing Pb-Tx design (e.g., mAb affinity, masking strength, and substrate stability), a reduced TMDD model such as the rapid equilibrium approximation would be a more parsimonious option and possibly sufficient for a subset of applications. The parameters k_{13} and k_{31} in the QSP Pb-Tx model were derived in part based on the assumed values of p[11,12] and Q[13,14]of 0.5 and 1e-5 1/second, respectively (see **Table 2**); this component of the QSP model could be modified to incorporate additional mechanistic information by explicitly using the Wittrup tumor equations,[13] or alternatively k_{13} and k_{31} could likewise be parametrized using the Wittrup tumor equations. Lastlu, additional information regarding substrate cleavage kinetics coupled with spatiotemporal protease activity data both across species and in normal and pathophysiological states could help to further refine the components of the model governing Pb-Tx activation for a more fully mechanistic treatment.

Supporting Information. Supplementary information accompanies this paper on the *CPT: Pharmacometrics & Systems Pharmacology* website (www.psp-journal.com).

Figure S1. Parametric study of (**a**) mask and (**b**) substrate.
Figure S2. Model-predicted net flux (nmol/second) of single and dual cleaved PROBODY therapeutics (Pb-Tx) from central, peripheral and tumor compartments.
Model code.

Acknowledgments. PROBODY is a trademark of CytomX Therapeutics, Inc.

Funding. The study was funded by CytomX Therapeutics, Inc., South San Francisco, CA.

Conflict of Interest. M.S., J.S., and W.M.K. are or were CytomX employees and own CytomX stock. J.M.B., J.F.A., L.L., and B.L.M. are Applied BioMath employees.

Author Contributions. M.S., J.S., J.M.B., J.F.A., and W.M.K. wrote the manuscript. M.S., J.S., J.M.B., J.F.A., and W.M.K. designed the research. M.S., J.S., J.M.B., J.F.A., and W.M.K. performed the research. J.M.B., J.F.A., L.L., B.L.M., M.S., J.S., and W.M.K. analyzed the data.

1. Buss, N.A., Henderson, S.J., McFarlane, M., Shenton, J.M. & de Haan, L. Monoclonal antibody therapeutics: history and future. *Curr. Opin. Pharmacol.* **12**, 615–622 (2012).
2. Desnoyers, L.R. *et al.* Tumor-specific activation of an EGFR-targeting probody enhances therapeutic index. *Sci. Transl. Med.* **5**, 207ra144 (2013).
3. Gibiansky, L. & Gibiansky, E. Target-mediated drug disposition model: approximations, identifiability of model parameters and applications to the population pharmacokinetic-pharmacodynamic modeling of biologics. *Expert Opin. Drug Metab. Toxicol.* **5**, 803–812 (2009).
4. Wang, W., Wang, E.Q. & Balthasar, J.P. Monoclonal antibody pharmacokinetics and pharmacodynamics. *Clin. Pharmacol. Ther.* **84**, 548–558 (2008).
5. Jain, R.K. Physiological barriers to delivery of monoclonal antibodies and other macromolecules in tumors. *Cancer Res.* **50**(3 suppl.), 814s–819s (1990).
6. Vicini, P. & van der Graaf, P.H. Systems pharmacology for drug discovery and development: paradigm shift or flash in the pan? *Clin. Pharmacol. Ther.* **93**, 379–381 (2013).
7. Uhlen, M., Fagerberg, L., Hallstrom, B.M., Lindskog, C., Oksvold, P., Mardinoglu, A. … Ponten, F. Proteomics. Tissue-based map of the human proteome. *Science* **347**(6220), 1260419 (2015). https://doi.org/10.1126/science.1260419.
8. Schlosshauer, M. & Baker, D. Realistic protein-protein association rates from a simple diffusional model neglecting long-range interactions, free energy barriers, and landscape ruggedness. *Protein Sci.* **13**, 1660–1669 (2004).
9. Bianconi, E. *et al.* An estimation of the number of cells in the human body. *Ann. Hum. Biol.* **40**, 463–471 (2013).
10. de Goeij, B.E. & Lambert, J.M. New developments for antibody-drug conjugate-based therapeutic approaches. *Curr. Opin. Immunol.* **40**, 14–23 (2016).
11. Baxter, L.T., Zhu, H., Mackensen, D.G. & Jain, R.K. Physiologically based pharmacokinetic model for specific and nonspecific monoclonal antibodies and fragments in normal tissues and human tumor xenografts in nude mice. *Cancer Res.* **54**, 1517–1528 (1994).
12. Deng, R. *et al.* . Preclinical pharmacokinetics, pharmacodynamics, tissue distribution & tumor penetration of anti-PD-L1 monoclonal antibody, an immune checkpoint inhibitor. *MAbs.* **8**, 593–603 (2016).
13. Thurber, G.M. & Dane Wittrup, K. A mechanistic compartmental model for total antibody uptake in tumors. *J. Theor. Biol.* **314**, 57–68 (2012).
14. Posey, J.A. *et al.* A phase I study of anti-kinase insert domain-containing receptor antibody, IMC-1C11, in patients with liver metastases from colorectal carcinoma. *Clin. Cancer Res.* **9**, 1323–1332 (2003).
15. Dong, J.Q. *et al.* Quantitative prediction of human pharmacokinetics for monoclonal antibodies: retrospective analysis of monkey as a single species for first-in-human prediction. *Clin. Pharmacokinet.* **50**, 131–142 (2011).
16. Davies, B. & Morris, T. Physiological parameters in laboratory animals and humans. *Pharm. Res.* **10**, 1093–1095 (1993).
17. Lauffenburger, D.A. & Linderman, J.J. Receptors: Models for binding, trafficking, and signaling. Oxford University Press, New York, NY (1993).
18. Parise, C.A., Bauer, K.R., Brown, M.M. & Caggiano, V. Breast cancer subtypes as defined by the estrogen receptor (ER), progesterone receptor (PR), and the human epidermal growth factor receptor 2 (HER2) among women with invasive breast cancer in California, 1999-2004. *Breast J.* **15**, 593–602 (2009).
19. Ryu, E.B., Chang, J.M., Seo, M., Kim, S.A., Lim, J.H. & Moon, W.K. Tumour volume doubling time of molecular breast cancer subtypes assessed by serial breast ultrasound. *Eur. Radiol.* **24**, 2227–2235 (2014).
20. Deng, R., Iyer, S., Theil, F.P., Mortensen, D.L., Fielder, P.J. & Prabhu, S. Projecting human pharmacokinetics of therapeutic antibodies from nonclinical data: what have we learned? *MAbs.* **3**, 61–66 (2011).